The Gas-rich Circumbinary Disk of HR 4049. II. A Detailed Study of the Near-infrared Spectrum

Article *in* The Astrophysical Journal · October 2013

DOI: 10.1088/0004-637X/780/1/41 · Source: arXiv

2 authors, including:

Jan Cami
The University of Western Ontario
146 PUBLICATIONS **1,978** CITATIONS

The Astrophysical Journal, 780:41 (9pp), 2014 January 1 doi:10.1088/0004-637X/780/1/41

THE GAS-RICH CIRCUMBINARY DISK OF HR 4049. I. A DETAILED STUDY OF THE MID-INFRARED SPECTRUM

S. E. Malek[1] and J. Cami[1,2]
[1] Department of Physics & Astronomy, University of Western Ontario, London, ON N6A 3K7, Canada;
sarahemalek@gmail.com, jcami@uwo.ca
[2] SETI Institute, 189 Bernardo Avenue, Suite 100, Mountain View, CA 94034, USA
Received 2013 May 21; accepted 2013 October 19; published 2013 December 11

ABSTRACT

We present a detailed analysis of the mid-infrared spectrum of the peculiar evolved object HR 4049. The full *Spitzer*-IRS high-resolution spectrum shows a wealth of emission with prominent features from CO_2 and H_2O and possible contributions from HCN and OH. We model the molecular emission and find that it originates from a massive ($M \gtrsim 8 \times 10^{-3}\ M_\odot$), warm ($T_{ex} \approx 500$ K) and radially extended gas disk that is optically thick at infrared wavelengths. We also report less enrichment in ^{17}O and ^{18}O than previously found and a comparison of the *Spitzer* observations to earlier data obtained by the Short Wavelength Spectrometer on board the *Infrared Space Observatory* reveals that the CO_2 flux has more than doubled in 10 yr time, indicating active and ongoing chemical evolution in the circumbinary disk. If the gas originates from interaction between the stellar wind and the dust, this suggests that the dust could be oxygen-rich in nature. The molecular gas plays a crucial role in the thermal properties of the circumbinary disk by allowing visible light to heat the dust and then trapping the infrared photons emitted by the dust. This results in higher temperatures and a more homogeneous temperature structure in the disk.

Key words: circumstellar matter – stars: AGB and post-AGB – stars: individual (HR 4049)

Online-only material: color figures

1. INTRODUCTION

HR 4049 is considered the prototype for a class of evolved objects with peculiar properties. Their effective temperatures and luminosities suggest that they are in the post-asymptotic giant branch (post-AGB) phase of their evolution, but their evolutionary path may be severely affected by the presence of a companion (see Van Winckel et al. 1995 for a review). Indeed, their unusual properties all seem to result from stellar evolution in a binary system.

Like many of the members of this class, HR 4049 shows a significant infrared (IR) excess and ultraviolet (UV) deficit (Lamers et al. 1986), suggesting the presence of a massive circumbinary disk. This disk is the result of mass loss in the binary system and plays a significant role in its unusual properties. For instance, the photospheric abundances of HR 4049 show an extreme depletion in refractory elements (e.g., [Fe/H] = −4.8, Waelkens et al. 1991b) while showing nearly solar abundances for volatiles (e.g., [S/H] = −0.2, [C/H] = −0.2, [N/H] = 0.0, [O/H] = −0.3 Takada-Hidai 1990; Waelkens et al. 1991b). This peculiar depletion pattern is the result of dust formation in the disk followed by accretion of the gas which is now devoid of refractory elements (Mathis & Lamers 1992; Waters et al. 1992). The circumbinary disk also causes HR 4049 to display photometric variability which is tied to its orbital period (Waelkens et al. 1991b).

Due to its importance in defining the characteristics of HR 4049, the dust component of the circumbinary disk has been the subject of a number of studies (e.g., Waelkens et al. 1991a; Dominik et al. 2003; Acke et al. 2013), revealing unusual dust properties. The infrared spectrum of HR 4049 does not show the dust features typically associated with circumstellar material around evolved stars (e.g., silicates or SiC) and thus the nature of the dust remains a mystery. Instead, the infrared excess is well-represented by a single temperature ($T \approx 1150$ K) blackbody from the onset of dust emission in the near-IR to submillimeter (submm) wavelengths. At the same time, the dust re-emits a significant fraction of the total stellar luminosity ($L_{IR} \approx L_*/3$), from which Dominik et al. (2003) deduced that HR 4049 is surrounded by an extremely optically thick and vertically extended disk with a hot inner wall. In this so-called wall model, the inner rim of the disk is 10 AU from the center of the binary system with a scale height of 3 AU and a temperature of 1150 ± 150 K.

However, Acke et al. (2013) found that the wall model was inconsistent with interferometric observations of HR 4049 which showed a radially extended disk. Instead, they proposed an optically thin dust disk composed of minerals without strong dust features—amorphous carbon being the most probable. In their model, the dust is slightly further from the center of the system and extends to much larger scale heights. Their model does not fit the spectral energy distribution (SED) beyond 20 μm, so they included a dust component composed of large grains at 200 K.

One potential clue to the nature of the dust (and the evolutionary status of the system) is the presence of strong emission features due to polycyclic aromatic hydrocarbons (PAHs; see Waters et al. 1989; Tielens 2008) as well as from nano-diamonds at 3.43 and 3.53 μm (Geballe et al. 1989; Guillois et al. 1999) and C_{60} (Roberts et al. 2012). Such species are often found in the environments surrounding evolved, carbon-rich objects, which suggests that HR 4049 may have once been a carbon star.

However, the IR spectrum also reveals a plethora of molecular bands from species that are more characteristic of oxygen-rich environments, but are very unusual nonetheless: Cami & Yamamura (2001) detected and identified the emission features due to all possible isotopologues of CO_2 containing ^{13}C, ^{17}O, and ^{18}O. Using optically thin models, they found that the gas was

extremely enriched in ^{17}O and ^{18}O (with $^{16}O/^{17}O = 8.3 \pm 2.3$ and $^{16}O/^{18}O = 6.9 \pm 0.9$). Subsequently, Hinkle et al. (2007) analyzed the first overtone and fundamental bands of CO in the near-IR spectrum and found no enrichment in ^{17}O and ^{18}O. Although they detected CO isotopologues containing ^{17}O and ^{18}O in the fundamental, they did not observe these isotopologues in the overtone. They attributed the discrepancy between their oxygen abundances and those detected by Cami & Yamamura (2001) to the optically thick nature of the CO_2 emission in the mid-IR observations.

A detailed study of the gas has been difficult thus far due to the low sensitivity of the observations taken with the Short Wavelength Spectrometer (SWS) on board the *Infrared Space Observatory* (*ISO*; de Graauw et al. 1996) as well as limitations in earlier line lists describing the transition energies and probabilities of the molecular species present in this spectrum. However, a good understanding of the gas composition should yield clues to the evolutionary history of this system as well as to the processing that occurs in these environments.

Here, we present observations from the Infrared Spectrograph (IRS; Houck et al. 2004) on board the *Spitzer Space Telescope* (Werner et al. 2004) which have a higher signal-to-noise (S/N) ratio as well as better spectral resolution. In addition, due to improvements in available line lists, we will be able to include the effects of optical depth in our spectral models.

In addition to the CO_2 bands, we analyze the other spectral features in the *Spitzer*-IRS and *ISO*-SWS spectra. We provide an inventory of the gas components and compare the observations to molecular model spectra to obtain excitation temperatures, column densities and optical depths. In turn, these numbers provide quantitative information on the gas disk which we compare to earlier studies of the dust in this object. We then compare our results from these analyses to the CO observations in the near-IR spectrum from Phoenix on Gemini in Malek & Cami (2013, hereafter Paper II).

This paper is organized as follows. In Section 2, we describe the observational data and reduction steps. We describe our modeling technique in Section 3 and present our results of this analysis in Section 4. Then we describe how these results fit with the other observations of the system in Section 5 and finally, we present our conclusions in Section 6.

2. OBSERVATIONS AND DATA REDUCTION

2.1. Spitzer-IRS

HR 4049 was observed at high spectral resolution ($R = 600$) using the IRS (Houck et al. 2004) aboard the *Spitzer Space Telescope* (Werner et al. 2004) in the short–high (SH; $\lambda = 9.9$–19.6 μm) mode (AOR key 4900608; program ID 93; PI: D. Cruikshank) and the long–high (LH; $\lambda = 18.7$ to 37.2 μm) mode (AOR key 23711232; program ID 40896; PI: J. Cami). For the LH data, we also obtained background observations (AOR key 23711488).

We used the SMART data reduction package (v8.2.2, Higdon et al. 2004) as well as custom IDL routines to carry out the data reduction. Starting from the basic calibrated data, we first cleaned all data with IRSCLEAN using the campaign rogue pixel mask. When we examined the LH background observations, we found the background flux levels were fairly low (typically less than 1% of the target flux with some small unresolved spikes up to 5% of the target flux) and featureless. We thus subtracted this background from the target observations. We then combined the cleaned data collection events for each observation using a weighted average. Next, we extracted the spectra from the SH data and the background subtracted LH data using full aperture extraction in SMART v8.2.2 (Higdon et al. 2004).

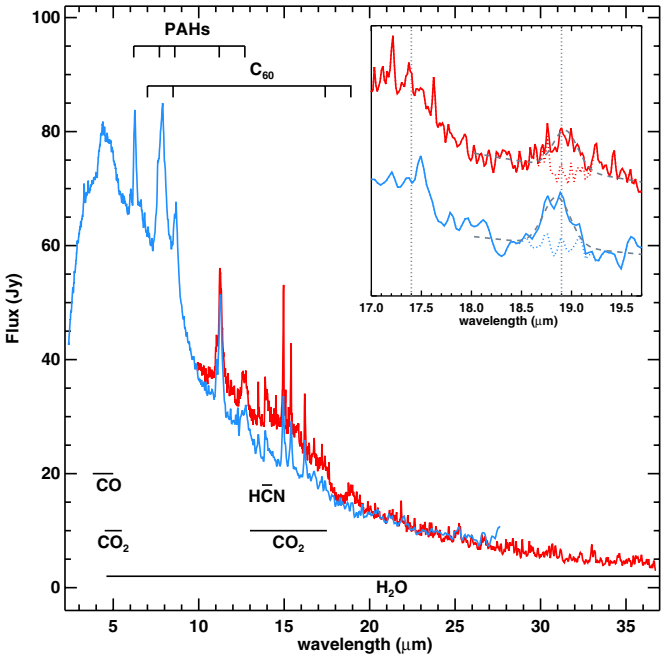

Figure 1. *Spitzer*-IRS (black, red in the online version) and speed 2 *ISO*-SWS (light gray, blue in the online version) observations of HR 4049 are shown. The polycyclic aromatic hydrocarbon (PAH) bands at 6.2, 7.7, 8.6, 11.2, and 12.7 μm are highlighted as well as the positions of the C_{60} bands at 7.0, 8.5, 17.4, and 18.9 μm. The regions of the spectrum showing emission from CO, CO_2, H_2O, and HCN are also highlighted. The inset shows the 17 to 19.5 μm region of the *Spitzer*-IRS (black, red in the online version) and speed 1 *ISO*-SWS spectra (light gray, blue in the online version) highlighting the locations of the 17.4 and 18.9 μm C_{60} bands and showing the best-fit Gaussians to the 18.9 μm bands (dashed gray lines) with the corresponding residuals for the fitting region (dotted lines).

(A color version of this figure is available in the online journal.)

We then defringed the extracted spectra and trimmed the edges of the orders. Flux differences between adjacent orders were typically on the order of 5% among the SH orders and only one LH order showed a notable flux difference. We scaled adjacent orders to the median flux in the overlap region, using order 11 ($\lambda_c = 18.7$ μm for SH and $\lambda_c = 35.4$ μm for LH) as the reference. We then compared the spectra in overlap regions as well as the two nod positions while checking for consistency, averaged them using a weighted mean, and rebinned the resulting final spectrum.

We compared the long wavelength end of the SH spectrum and the short wavelength end of the LH spectrum and calculated a weighted mean for the overlap region. Finally, we scaled the *Spitzer*-IRS spectrum to the *Infrared Astronomical Satellite* (*IRAS*) flux measurement at 25 μm (scaling up by 50%). The final spectrum is presented in Figure 1.

2.2. ISO-SWS

HR 4049 was observed twice with the SWS (de Graauw et al. 1996) aboard the *ISO* (Kessler et al. 1996): on 1995 December 27 (AOT 1, speed 1) and again on 1996 May 6 (AOT 1, speed 2); both observations correspond to a resolving power of ~300. Here, we use the speed 2 *ISO*-SWS data that was also presented by Cami & Yamamura (2001) and Dominik et al. (2003).

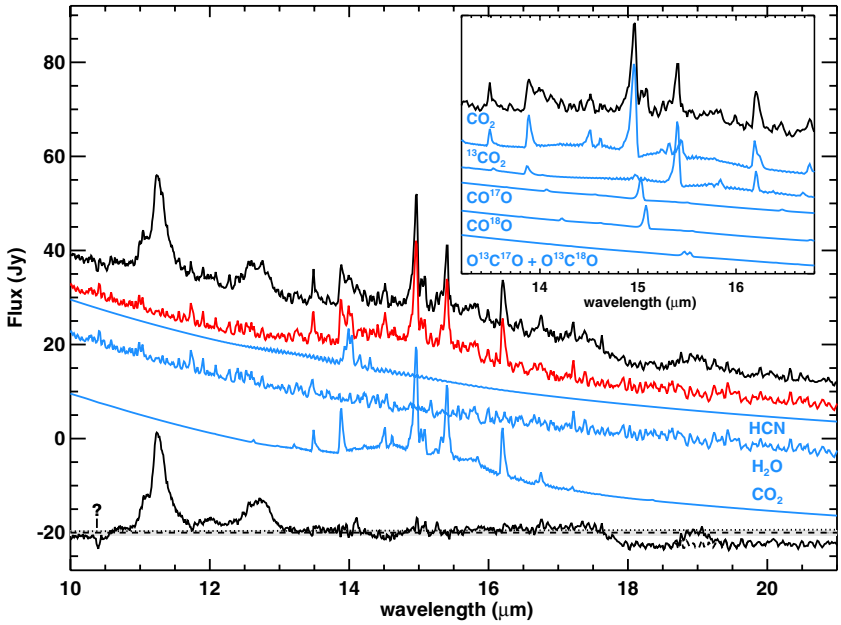

Figure 2. *Spitzer*-IRS spectrum between 10 and 20 μm (black) with the best fit model for all the molecules (dark gray or red in the online version) offset below the spectrum and models of the individual molecules below that (gray or blue in the online version) in descending order: HCN, H_2O, and CO_2. The residual without the linear component is shown at the bottom of the figure in black with the error values on the data indicated in light gray. We also fit a Gaussian to the C_{60} feature at 19 μm in the residual and show the effect of removing this Gaussian in dashed lines. The inset shows a breakdown of the CO_2 isotopologues between 13 and 17 μm.

(A color version of this figure is available in the online journal.)

We compare the speed 2 *ISO*-SWS spectrum to the *Spitzer*-IRS observations in Figure 1. At the longer wavelengths, the spectra agree well with one another; however, the *Spitzer*-IRS data exhibit a significant increase in the flux levels between 10 and 18 μm.

3. ANALYSIS

Figure 1 shows the full *Spitzer*-IRS spectrum with emission from a variety of molecular species indicated. There are prominent features from large molecules such as PAHs (Waters et al. 1989) and C_{60} (Roberts et al. 2012). We have also indicated the broad emission features from CO_2 at 15 μm, the HCN feature at 14 μm and the region of the spectrum where we observe H_2O emission. There is also emission from CO and CO_2 at 4.6 and 4.2 μm, respectively, in the *ISO*-SWS spectrum.

3.1. Modeling the Spitzer Spectrum

To determine the properties of the gas in the mid-IR spectrum of HR 4049 and fully characterize the molecular emission, we created model spectra and compared them to the observational data. We used the same methods employed to build the SpectraFactory database (Cami et al. 2010b). For each model, we began with line lists detailing the frequencies and intensities of individual molecular transitions. We calculated optical depth profiles from the line lists assuming a population in local thermodynamic equilibrium (LTE) and a Gaussian intrinsic line profile with a width of 3 km s^{-1}. We summed the optical depth profiles for the different molecular species (including isotopologues) and then performed the proper radiative transfer calculations through an isothermal slab and smoothed the resulting model spectrum to match the SH resolution ($R = 600$).

We used a 1150 K blackbody for the continuum and applied a non-negative least-squares (NNLS) algorithm (Lawson & Hanson 1974) with the continuum and the molecular emission models as parameters. Then we compared our model to the observational data between 13.27 and 18 μm (to cover the CO_2 emission) and calculated χ^2_ν, the reduced χ^2 statistic for each model to determine the quality of the fit.

We experimented with several different models to determine the best range for each of our parameters then selected the parameters for each model using an adaptive mesh algorithm. In our final fits, we varied the temperature of the molecular layer between 200 and 1000 K in increments of 100 K and column densities between 10^{16} and 10^{22} cm^{-2} in increments of $\log N = 0.2$ for all molecules in this region. Additionally, we varied $\log(^{12}C/^{13}C)$ from 0 to 2; $\log(^{16}O/^{18}O)$, $\log(^{16}O/^{17}O)$, and $\log(^{14}N/^{15}N)$ from 0 to 3 in increments of 0.2.

While we began fitting only CO_2 and its isotopologues, we later included H_2O and HCN in our model spectra. In addition, we noted a small linear trend in our residuals from 13 to 17.5 μm. We do not know the origin of this trend, but we incorporated a linear component in our NNLS routine to compensate for this residual.

4. RESULTS

We present the parameters for our best fit model in Table 1 and the 10 to 20 μm region of the *Spitzer*-IRS spectrum with our best fit model in Figure 2. We focus on the H_2O emission at LH wavelengths in Figure 3 and we compare the models to the full spectrum *Spitzer*-IRS and our predictions at *ISO*-SWS wavelengths in Figure 4. We find a χ^2_ν of 3.5 for the fit to the *Spitzer*-IRS observations and a good representation of the molecular emission features within our fitting region.

When we compare the predictions from our model at longer and shorter wavelengths to the spectrum, we find that the spectral features are also fit remarkably well. The majority of the molecular features in the LH spectrum, for example, appear to be from H_2O emission. In addition, the spikes on the PAH features at 11.2 and 12.7 μm disappear and some of the smaller PAH features become evident.

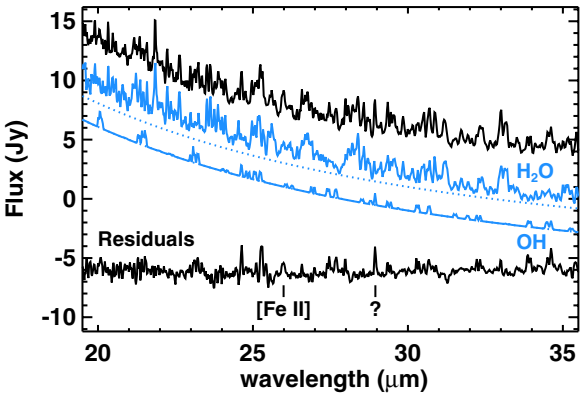

Figure 3. *Spitzer*-IRS spectrum of HR 4049 (black) with the best fit model for H_2O and a model for OH at the same temperature and column density offset below the spectrum (gray or blue in the online version). The dotted gray (blue in the online version) lines indicate the blackbody continuum under the H_2O and OH models.

(A color version of this figure is available in the online journal.)

Table 1
Temperatures, Column Densities, and Isotope Ratios for the Best Model Fits to the Data as Well as the Nominal 3σ Uncertainties

	Spitzer-IRS	*ISO*-SWS
λ_{fit} (μm)	13.7–18	2.4–5.8; 9.5–10.5; 14–22
Temperature (K)	500 ± 50	600 ± 50
log N (CO_2)	19.0 ± 0.1	17.8 ± 0.1
log N (H_2O)	$21.6^{+0.1}_{-0.2}$	19.4 ± 0.1
log N (HCN)	17.8 ± 0.1	...
log N (CO)	...	22.0 ± 0.1
$^{12}C/^{13}C$	6^{+2}_{-1}	$1.6^{+2}_{-0.4}$
$^{16}O/^{17}O$	160^{+90}_{-35}	40^{+23}_{-9}
$^{16}O/^{18}O$	160^{+40}_{-60}	16^{+4}_{-3}
$^{14}N/^{15}N$	13^{+3}_{-8}	...

4.1. CO_2

The *Spitzer*-IRS spectrum shows prominent emission from the CO_2 isotopologues observed by Cami & Yamamura (2001) in addition to others (e.g., the $O^{13}C^{17}O$ and $O^{13}C^{18}O$ peaks which Cami & Yamamura 2001 were unable to separate due to the lower spectral resolution of *ISO*-SWS). To model the emission from CO_2, we used line lists from the 1000 K Carbon Dioxide Spectroscopic Database (Tashkun et al. 2003) including the $^{13}CO_2$, $CO^{17}O$, $CO^{18}O$, $O^{13}C^{17}O$, and $O^{13}C^{18}O$ isotopologues.

Though our single layer LTE model reproduces the majority of the CO_2 features very well, (see Figure 2), we find that the best fit model tends to slightly overestimate the flux relative to the local continuum between 14.2 and 14.7 μm while underestimating the flux between 16.7 and 17.6 μm (which may be due to some contribution from C_{60} at the long wavelength end). We also find high optical depths across most of our fit region with this model.

There are also small spikes which may be due to a slight temperature stratification in the CO_2 layer. For example, we note a small feature in the residual spectrum at 16.64 μm which could be due to the transition between the $4\nu_2^4$ and $3\nu_2^1$ levels, which suggests the presence of additional hotter gas. We also observe a small residual peak at 14.98 μm near the main CO_2 band, which is a combination of the ν_2 bending mode at 14.98 μm ($1\nu_2^1$ to the ground state) and subsequent hot bands which are each shifted slightly to the blue; the presence of residual emission at 14.98 μm thus suggests the presence of some colder CO_2. The high optical depths of the gas could make the appearance of the bands more sensitive to these types of temperature variations; however, these residuals are relatively small, suggesting that most of the emission originates from a relatively thermally homogeneous layer.

We also note some small residual emission at 15.04 and 15.10 μm, which could be due to additional emission from the main ν_2 bands of the $OC^{17}O$ and $OC^{18}O$ isotopologues respectively.

4.2. H_2O and OH

After including all CO_2 isotopologues in our models, many weaker emission features remained in the residuals of this region. We noticed that several features are consistent with emission from water vapor. Thus, we recalculated our models including optical depth profiles for H_2O using line lists from Partridge & Schwenke (1997, including the $H_2^{17}O$ and $H_2^{18}O$ isotopologues).

We find an extremely high column density for H_2O and a much better correspondence to the results than for CO_2, not only in the region we chose to fit, but also at longer and shorter wavelengths in the *Spitzer*-IRS spectrum. Upon careful examination of the residuals in Figure 2, one may note that the spikes atop the 11.2 and 12.7 μm PAH features disappear almost completely and remarkably, the 12 μm PAH feature becomes apparent though it was previously hidden by H_2O emission. Furthermore, the 18.9 μm C_{60} feature becomes much more prominent and clear when H_2O emission is removed. In Figures 3 and 4, it is also clear that H_2O accounts for the bulk of the features in the LH spectrum since the residuals contain relatively few remaining spectral features. This observation also confirms the earlier detection of water in HR 4049 in the near-IR by Hinkle et al. (2007).

Since OH was also detected by Hinkle et al. (2007) at $\sim$3 μm, and since it has many features in this wavelength range, we included it in our models between 13.24 and 18 μm. However, we were unable to detect OH in this region of the spectrum. We were also unable to fit any OH using only H_2O and OH between 20 and 35 μm. In Figure 3, we show a comparison between model spectra of H_2O and OH using the same temperatures and column densities at LH wavelengths. We note that while there appear to be many features in our residuals which are consistent with emission from OH, it is not possible to reliably fit the OH features due to extensive contamination from H_2O.

4.3. HCN

When all the CO_2 and H_2O isotopologues are included in our models, there is still significant residual emission at 14.04 μm, where the CH bending mode of HCN is often seen in evolved stars. Indeed, the SpectraFactory catalogue (Cami et al. 2010b) reveals a clear HCN molecular band at this wavelength, thus we include it in our model calculations using line lists from the HITRAN 2008 database (Rothman et al. 2009, including the $H^{13}CN$ and $HC^{15}N$ isotopologues).

We determine a column density for HCN which is much lower than that of CO_2 and H_2O ($\log N = 17.8$), which suggests that it is less abundant. We included isotopologues of HCN containing ^{13}C and ^{15}N which appear slightly to the red of the

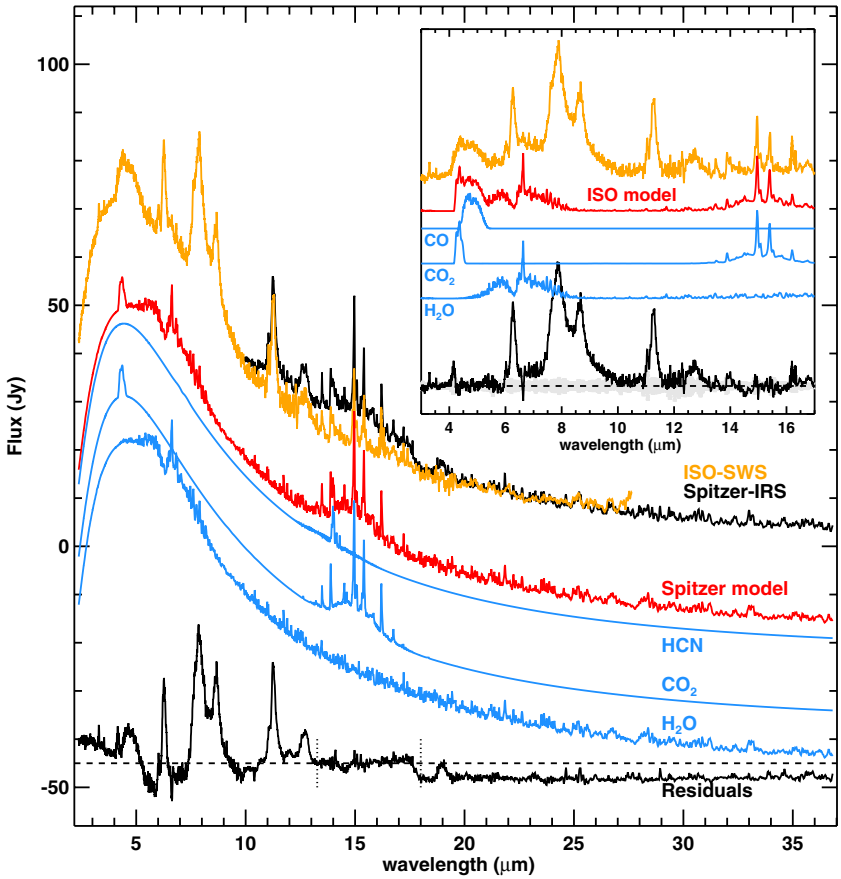

Figure 4. Main plot: *Spitzer*-IRS spectrum (black) and *ISO*-SWS spectrum (light gray or orange in the online version) for HR 4049 with the best fit model (dark gray or red in the online version) to the *Spitzer*-IRS spectrum and models for the individual components for CO_2, H_2O, and HCN offset below the spectrum (gray or blue in the online version) as well as the residuals (black). The vertical dotted lines indicate the region of the spectrum used to fit the model to the *Spitzer*-IRS data. The model outside of these wavelength ranges (including the *ISO*-SWS spectrum) is the prediction based on these best fit parameters. Inset: model fit to the *ISO*-SWS spectrum, with the best fit model (dark gray or red in the online version) and individual components for CO, CO_2, and H_2O offset below the spectrum (gray or blue in the online version). The residuals for this model are shown in black and the uncertainties in the data are shown in light gray.

(A color version of this figure is available in the online journal.)

main isotopologue and are thus able to find $^{14}N/^{15}N$ of 13^{+3}_{-5}. With only one band containing this isotope though, we do not consider our ratio here to be especially reliable.

4.4. Fullerenes

Since its detection in the young planetary nebula Tc 1 by Cami et al. (2010a), C_{60} has been reported in other evolved binary systems (Gielen et al. 2011b) and it was recently reported in HR 4049 by Roberts et al. (2012), who detected the 17.4 and 18.9 μm features.

Indeed, the 18.9 μm feature is clear (and also present in the *ISO*-SWS speed 1 observations, see the inset of Figure 1) and when we subtract our best fit H_2O model, the feature becomes much more prominent (see Figure 2). Fitting the 18.9 μm C_{60} feature in the residual spectrum with a Gaussian, we determine a FWHM of 0.40 μm and a central wavelength of 18.98 μm. This is a much narrower band than found by Roberts et al. (2012), who reported a FWHM of 0.64 μm. This difference may be due to the presence of the water features, which makes the band appear broader.

The 17.4 μm feature is buried in the optically thick CO_2 emission, so we cannot measure it accurately. Additionally, since no observations were taken by the IRS short low (SL; $R = 90$ to 127, $\lambda = 5.2$ to 14.5 μm) mode, the 7 and 8.5 μm features for C_{60} would only appear in the *ISO*-SWS spectrum. However, we do not see them, which could be due to a combination of the sensitivity of *ISO*-SWS and the often weak nature of these features.

4.5. PAHs

The spectral region covered by the *Spitzer*-IRS observations covers only the 11.2 and 12.7 μm PAH features. These bands also appear in the *ISO*-SWS spectrum alongside features at 6.2, 7.7 and 8.6 μm. The PAH features in the *ISO*-SWS spectrum of HR 4049 were described in detail by Beintema et al. (1996) and Molster et al. (1996) and are class B (Peeters et al. 2002).

Examining the residual spectra (see Figure 2 especially), we note that some of the less prominent PAH features become clear when the H_2O emission is removed from the spectrum. For instance, the 12 μm feature from CH out-of-plane duo-modes and the weak, broad feature at 10.7 μm from PAH cations (Hony et al. 2001) are not clear in the original spectrum, but stand out in the residual. In addition, we find that the profiles of the already prominent PAH features become clearer when the H_2O emission is removed.

4.6. Residual Features

There are a few interesting features in the residual spectrum. For instance, we note a small absorption feature at 10.38 μm. This feature was previously observed in the carbon-rich

pre-planetary nebula SMP LMC 11 by Malek et al. (2012), who suggested that this feature is molecular in nature, but they were unable to identify the carrier.

As described above, a few of the residual features in the LH spectrum may be due to OH emission. However, we also observe an emission feature at 25.99 μm which could be due to a fine-structure line from [Fe II] (see Figure 3). To confirm that this feature is real, we examined the background observations and determined that this region of the spectrum was featureless. Then we examined both nod positions in the background-subtracted spectrum and noted that it appeared in both.

This transition is from the $J = 7/2$ to $J = 9/2$ (ground) level in the a^6D state. The next transition would appear at 35.35 μm ($J = 5/2$ to $J = 7/2$), but we do not observe a clear feature from this line. Instead, we observe a large and broad spike which appears to be from noise (S/N decreases toward the end of the LH spectrum). If we assume that the [Fe II] is at the same temperature as the molecular layer (500 K), we can estimate the strength of the expected emission at 35.35 μm. Using the method described in Justtanont et al. (1999), we find that the 35.35 μm line should be 80% as strong as the 25.99 μm line, which could be hidden by this spike in the noise.

Plateau emission. In addition to the small emission features in our residuals, we note that we are unable to properly reproduce the continuum beyond ~17.6 μm. Indeed, examining Figures 2 and 4, we see that we systematically overestimate the continuum emission at LH wavelengths. As well, we note that one of the major differences between the *Spitzer*-IRS and *ISO*-SWS spectra in Figure 1 is the presence of emission from a continuum-like "plateau" under the CO_2 emission in the *Spitzer* spectrum.

If we force the dust continuum to represent the LH continuum more accurately, we find that our models cease to reproduce the narrow emission bands from CO_2. If we instead fit the narrow emission features, we overestimate the dust continuum at LH wavelengths. We have chosen to use a model which reproduces the narrow CO_2 features, but we note that the dust continuum from our best fit model is much higher than it should be as a result.

Part of this plateau emission is likely due to the presence of C_{60}. However, since the residual flux is much wider than the 17.4 μm C_{60} feature, this will not account for all of this plateau. In addition, the carrier of this plateau emission appears to have formed between the observations by *ISO* and *Spitzer* since this is perhaps the most obvious difference between the two spectra. We therefore considered two possible sources for this plateau emission.

First, we considered the possibility that this could be due to broad PAH emission from C–C–C bending modes, which has been observed to form a continuum between 15 and 20 μm (e.g., Van Kerckhoven et al. 2000; Boersma et al. 2010). These PAH plateaus also often show narrow features at 16.4, 17.4 and 18.9 μm along with a weak 15.8 μm feature (Tielens et al. 1999; Moutou et al. 2000). However, we do not see any obvious PAH features to the red of the 12.7 μm feature. Therefore, we consider it unlikely that this plateau is due to PAH emission.

Another possible candidate for this plateau emission is CO_2. While our CO_2 models predict some continuum-like emission, it is not enough to match the plateau we observe. We do find high optical depths for CO_2 ($\tau_{max} \approx 160$ for the main isotopologue using a line width of 3 km s^{-1}, this would decrease to $\tau_{max} \approx 52$ for 10 km s^{-1}) as well as some evidence for temperature stratification in the residuals and possibly recent CO_2 formation which could result in some non-LTE emission. We therefore consider that the plateau emission could be due to CO_2 emission that our models are unable to fit properly. We will explore this possibility further in Section 5.4. We note that a similar plateau was also observed in IRAS 06338 (Gielen et al. 2011b) and was attributed to optically thick CO_2 emission.

4.7. ISO Spectrum

CO_2, H_2O, and HCN potentially all have features at the shorter wavelengths covered by *ISO*-SWS in addition to the features we observe in the *Spitzer*-IRS spectrum. We thus decided to compare the predictions from our model at these wavelengths to the *ISO*-SWS spectrum. We extended our model spectra to shorter wavelengths and smoothed the spectrum covered only by the *ISO*-SWS spectrum to a resolution of 300 to match these data. We present our prediction for these bands in the main plot of Figure 4.

These predictions do not appear to fit the *ISO*-SWS spectrum on first sight. However, some of the features do appear to be reproduced. Examining the CO_2 feature at 4.2 μm, we note that this band is heavily blended with the much broader CO emission band at 4.6 μm. It appears, however, that the CO_2 feature within this broader band is reproduced reasonably well.

If we examine our predictions for the H_2O spectrum, there is a broad emission feature between 5 and 8 μm. It is difficult to assess how well this broad band reproduces the spectrum in these regions due to the presence of the CO emission feature and the PAH features. However, our model predicts a fairly strong H_2O feature at 6.62 μm which is much weaker in the *ISO*-SWS spectrum.

Finally, although HCN also has an overtone mode at ~7 μm, our models do not predict it at these temperatures and column densities.

Since the *ISO*-SWS spectrum has a much larger wavelength coverage, it covers additional molecular bands (such as the 4.2 μm CO_2 feature) and species (CO at 4.6 μm), so we decided to fit this spectrum as well. We used the same techniques described for fitting the *Spitzer*-IRS spectrum, but we included CO in our model (using line lists from Goorvitch 1994, including the ^{13}CO, $C^{17}O$ and $C^{18}O$ isotopologues) and excluded HCN. We fit the spectrum in several regions to include as many molecular features as possible while excluding features we cannot fit (e.g., the PAHs). Thus, we used three fitting regions, first, between 2.4 and 5.8 μm, then from 9.5 to 10.5 μm and finally from 14 to 22 μm.

The parameters for our best fit are presented in Table 1 and this model is compared to the 3–17 μm region of the *ISO*-SWS spectrum in the inset of Figure 4. In our direct fit to the *ISO*-SWS spectrum, we find that the fit in the 4 μm region is greatly improved with the addition of CO and a more appropriate scaling factor for the continuum. However, we note that there are still issues in the H_2O emission at 6.62 μm where we fit a large emission spike which does not appear in the spectrum. In addition, there are some residuals at ~16 μm.

Time dependence. When we compare the *ISO*-SWS and *Spitzer* observations, we find that there is a dramatic increase in emission between 10 and 18 μm. If we subtract a 1150 K blackbody continuum from each spectrum and integrate the remaining flux between 13.4 and 16.8 μm, we find that the flux from molecular emission has more than doubled in this region between the time of the *ISO* and *Spitzer* observations (from $\sim 2 \times 10^{-10}$ W m^2 to $\sim 5 \times 10^{-10}$ W m^2).

5. DISCUSSION

The better quality of the *Spitzer*-IRS data and current line lists allow a much more in-depth analysis of the gas than was previously possible. As we shall see, many of the results of this analysis have important consequences for the properties of the circumbinary disk.

5.1. Isotopic Ratios

We remind the reader that in the optically thin limit, Cami & Yamamura (2001) determined that HR 4049 was extremely enriched in ^{17}O and ^{18}O ($^{16}O/^{17}O = 8.3 \pm 2.3$; $^{16}O/^{18}O = 6.9 \pm 0.9$). In a subsequent study of the near-IR CO bands, Hinkle et al. (2007) found isotopic ratios consistent with solar values and they suggested that the ratios determined by Cami & Yamamura (2001) were incorrect because the CO_2 emission in HR 4049 is actually optically thick. Based on our models, we are able to confirm the suggestion by Hinkle et al. (2007) that the CO_2 is optically thick, but we determine a ratio of 160^{+90}_{-35} for $^{16}O/^{17}O$ and 160^{+40}_{-60} for $^{16}O/^{18}O$, indicating some enrichment in ^{17}O and ^{18}O relative to solar values ($^{16}O/^{17}O = 2700$, $^{16}O/^{18}O = 479$, Anders & Grevesse 1989; Scott et al. 2006). In addition, these isotopes are enriched relative to typical AGB stars (where both are on the order of a 10^2 to 10^3; see Harris & Lambert 1984; Harris et al. 1985b, 1987, 1988; Smith & Lambert 1990). Indeed, the enrichment of ^{17}O and ^{18}O in HR 4049 appears to be similar to that of the Ba star HD 101013 ($^{16}O/^{17}O = 100^{+100}_{-50}$, $^{16}O/^{18}O = 60^{+100}_{-30}$, Harris et al. 1985a).

There are also recent detections of $OC^{18}O$ in two other binary post-AGB objects: EP Lyr and HD 52961 which both show enrichment in ^{18}O ($^{16}O/^{18}O$ of 19 for EP Lyr and 100 for HD 52961, Gielen et al. 2009). As well as a study of ^{18}O enrichment in R Coronae Borealis stars in which $^{16}O/^{18}O$ ratios less than one were found (Clayton et al. 2007).

We also note that the values we find here for the enrichment of ^{17}O and ^{18}O are more suitable to the scenario proposed by Lugaro et al. (2005) who suggested that the isotopic ratios for oxygen in HR 4049 could be due to nova nucleosynthesis; though HR 4049 lacks the UV flux for a typical white dwarf companion (Monier & Parthasarathy 1999). However, due to the high optical depths we find, our values are poorly determined and our uncertainties on these values are likely to be larger than we find from our models. We also suggest that there may be similar issues with the $^{16}O/^{18}O$ values in the other post-AGB objects for the same reason.

Our best fit models appear to indicate an enrichment in ^{13}C, with $^{12}C/^{13}C$ of 6^{+2}_{-1}. This relatively low value agrees with an early termination of the AGB due to accelerated mass loss along the orbital plane of the binary (Iben & Livio 1993). This has been observed in other binary post-AGB objects such as EP Lyr (Gielen et al. 2008). However, optically thick CO_2 emission also makes this ratio uncertain.

5.2. Gas Distribution and Disk Structure

From our models, we find that not only is the CO_2 emission optically thick, but the gas is optically thick across the entire spectrum (e.g., $\tau > 10$ for H_2O across the entire *Spitzer*-IRS spectrum). This has some very important ramifications. For instance, when the gas is optically thick, the flux will scale with the emitting area, thus we are able to estimate the spatial extent of the gas using our models.

When we calculate our models, we obtain a scale factor (f) which relates I_ν from our radiative transfer calculations to F_ν. We are able to relate this scale factor to the surface area (A) of the emitting layer such that $f = A/4D^2$, where D is the distance to HR 4049.

From our model fit to the *Spitzer*-IRS data, we find a value of 1.60×10^9 for f. If we use a distance of 640 pc for HR 4049 (as described by Acke et al. 2013), this scale factor corresponds to a projected area of 1117 AU^2. If we perform the same analysis using our best fit to the *ISO*-SWS spectrum (with $f = 1.57 \times 10^9$), we find a projected area of 1097 AU^2, which agrees reasonably well with the emitting region we estimate from our *Spitzer*-IRS data. Since the scale factors we determine have not changed much between the *ISO* and *Spitzer* observations despite the differences in column densities between the two models, this also supports our claim of optically thick gas.

If we then assume an inclination angle of 60° (which is agreed upon by both current models for the disk), we find an actual emitting surface of 1290 AU^2 for our molecular emission. If we consider how this surface area would fit into the current disk models, we note that this would not fit on the inner rim of the wall model.

This suggests that the gas belongs to a radially extended disk instead. If we assume that the gas exists some distance from the center of the binary system, we can estimate the maximum extent of the disk. Were the gas to originate 10 AU from the binary (as the dust in the wall model, Dominik et al. 2003), it would extend to a distance of 23 AU. If the gas begins at 15 AU from the binary (based on the interferometric observations by Acke et al. 2013), it would extend to 25 AU, a distance which agrees well with the maximum radial extent of the disk determined from the interferometric observations by Acke et al. (2013).

It would be reasonable to suppose that the gas is mixed in with any dust in the circumbinary disk of HR 4049. As described by Dominik et al. (2003), dust grains in a gas-rich disk tend to settle toward the midplane of the disk, so the gas we observe could form a sort of atmosphere on the outside of the disk. There could also be more gas inside the disk which we are unable to observe since this atmosphere is optically thick. However, the gas on the inside of the disk could contribute to the opacity of the disk by providing some continuum-like emission similar to that we observe in our models.

As the LTE models reproduce the emission spectrum well and the gas appears to be reasonably warm (500 K), we find that we cannot reconcile our observations to a wall-type model for the dust. The wall model contains cold dust beyond the inner rim of the disk (Dominik et al. 2003), which would result in cold gas in this region. Instead, we observe a large region of warm gas so we find this sort of model improbable.

It would also be difficult to reconcile our observations to the disk model presented by Acke et al. (2013) in which the dust is optically thin. Acke et al. (2013) include gas in their disk to determine the scale height, however, CO_2 and H_2O are both excellent at trapping infrared radiation, especially at high column densities like those we observe in this disk and these effects are not included in their model.

Since these molecules are largely transparent at optical wavelengths, the stellar radiation will warm the dust grains. These grains will then re-emit this radiation in the infrared which will be absorbed and re-emitted by the gas in the disk, effectively trapping the radiation inside the disk. This will not only have the effect of warming the disk overall, but it will also keep the temperature relatively homogenous throughout the disk. Thus the disk could have the sort of narrow temperature range suggested by Dominik et al. (2003), who determined that

the SED of HR 4049 can be fit either by a 1150 K blackbody or by the sum of several equally weighted black bodies within a range of 880 K $\leqslant T \leqslant$ 1325 K.

However, in LTE, a gas cannot appear in emission in front of a hotter background source. Thus, we will explore alternate excitation mechanisms which could result in bands which emit in a way which appears similar to LTE in Section 5.4.

5.3. Total Gas Mass

Using the projected size for the emitting region and our column densities, we can estimate lower limits for the masses of the molecular species we observe in this system. Then, combining these with photospheric abundances, we can estimate a lower limit for the total mass of the gas in the circumbinary environment of HR 4049.

From our model fit to the *Spitzer*-IRS data, we calculate a mass of $9.19 \times 10^{-8}\ M_{\odot}$ for CO_2, $1.50 \times 10^{-5}\ M_{\odot}$ for H_2O, and $3.56 \times 10^{-9}\ M_{\odot}$ for HCN. Similarly, for the *ISO*-SWS model, we find masses of $5.69 \times 10^{-9}\ M_{\odot}$ for CO_2, $9.28 \times 10^{-8}\ M_{\odot}$ for H_2O, and $5.74 \times 10^{-5}\ M_{\odot}$ of CO.

Since the gas is oxygen-rich, we use the carbon abundance determined by Waelkens et al. (1991b, $\log N_C/N_H = 8.41-12$) along with the number of carbon-containing molecules and determine a lower limit for the total gas mass of $7.98 \times 10^{-3}\ M_{\odot}$ in the disk. This estimate is higher than the mass estimated by Dominik et al. (2003), who estimated $2.85 \times 10^{-4}\ M_{\odot}$ for the total mass of the disk. This could indicate a higher gas to dust ratio in the disk (they use a value of 100) or the presence of even more dust in this system than predicted by the wall model. If we compare our estimate for the gas mass to the dust mass from Acke et al. (2013, in which $M_{\rm dust} = (1.0 \pm 0.4) \times 10^{-8} M_{\odot}$), we find a gas-to-dust ratio of approximately 10^6. This appears unreasonably high, however this is the estimated mass for only the small grains in the disk, which are responsible for the near- and mid-IR SED as well as the optical and UV extinction. Their model also includes a cold dust component to reproduce the flux at the far-IR and submm wavelengths, which would contain more mass.

Since the gas is optically thick, this estimate will not include all the gas in the system (e.g., any gas beyond the optically thick layer or on the side of the disk inclined away from us is not included). In addition, since the majority of the gas included in our estimate is CO which only appears in the *ISO*-SWS spectrum, this may not describe the current gas mass since, as we will describe presently, it appears there is significant ongoing gas formation in HR 4049.

5.4. Time Evolution

It is somewhat surprising to see that the CO_2 flux has increased by a factor of 2.5 between the *ISO*-SWS and *Spitzer*-IRS observations (see Section 4.7). Since we scaled the *Spitzer*-IRS observations to match the *IRAS* flux point at 25 μm, we considered that this could be an issue in our comparison of these observations. However, the *ISO*-SWS spectrum was also scaled to the same point so this is unlikely to change our observation. Furthermore, it is not just the flux that has changed under the CO_2 emission features, but also the shape of the "continuum" and features in this region. Thus, it appears that the change in the emission features is real.

We compared the phase between the two observations using the phase information from Bakker et al. (1998). The SH observations were taken at a phase (ϕ) of 0.844, while the *ISO*-SWS speed 2 observations were taken at $\phi = 0.041$, near the photometric minimum. There are also the *ISO*-SWS speed 1 observations available, which were taken at a similar phase as the *Spitzer*-IRS observations ($\phi = 0.738$).

We thus compared the two *ISO*-SWS observations to see if there was a change in this region of the spectrum which could be attributed to phase. When we did so, we found that the spectra of the speed 1 and speed 2 *ISO*-SWS observations were roughly the same within the uncertainty measurements on the fluxes.

Thus, we conclude that the amount of emitting CO_2 gas we can observe has increased between the observations by *ISO*-SWS and those by *Spitzer*-IRS observations. If the gas were optically thin, this would imply that CO_2 has been forming at a rate of $3.68 \times 10^{-9}\ M_{\odot}\ \mathrm{yr}^{-1}$ assuming a constant formation rate. We note that this represents a considerable and rapid increase in CO_2 in the system, however, as we discovered, the CO_2 emission in the mid-IR spectrum is not optically thin so this represents a lower limit to the increase in CO_2. In addition, we cannot know whether the formation has been constant between the observations so this is a crude estimate for the formation rate.

While Bakker et al. (1996) reported a mass-loss rate from HR 4049 of $(6 \pm 4) \times 10^{-7}\ M_{\odot}\ \mathrm{yr}^{-1}$, the amounts of carbon and oxygen in the stellar winds are insufficient to permit the formation of so much new material. Therefore, we consider that the CO_2 we observe is forming from the interaction between the stellar wind and the dust disk.

The ongoing formation of oxygen-rich gas thus suggests that the dust contains an oxygen-rich component (e.g., silicates) and the absence of features from these dust species in the spectrum would therefore be due to obscuration of these features by optically thick gas; or by the dust being optically thick or perhaps being composed of large dust grains which have a smooth opacity. If the dust is primarily oxygen-rich, then HR 4049 would also be consistent with other post-AGB binaries in this regard (e.g., Gielen et al. 2011a).

While this may appear to be inconsistent with the fact that small dust grains are required to explain the optical and UV extinction, it was noted by Dominik et al. (2003) that the extinction at short wavelengths and the IR excess do not need to be caused by the same population of dust grains. Thus, although the optical and UV extinction is described well by a population of small grains of amorphous carbon or metallic iron as described by Acke et al. (2013), these grains cannot be the only dust component in the disk since they cannot allow the formation of the oxygen-rich gas we observe here.

The presence of small carbonaceous grains in the upper region of the disk could thus contribute to the extinction at short wavelengths while a population of oxygen-rich grains could contribute to part of the IR emission.

The evidence for ongoing formation of gas in the circumbinary disk of HR 4049 also suggests that the molecules are not actually in LTE, and the emission we observe may be due to pumping—either *radiative* pumping or *formation* pumping. In both cases, pumping results in a large fraction of molecules in highly excited vibrational states, either through absorption of higher energy photons (near-IR or even UV) or alternatively as a direct result of the formation of the molecules which leaves them in the excited states. After being pumped, they cascade down by emission of the IR photons we observe. Pumping would thus always produce emission at mid-IR wavelengths even when in front of hot dust. Superficially, such emission spectra could resemble LTE models; their main difference would be the

presence of many bands from higher vibrational levels. This could help explain the plateau emission as a forest of CO_2 emission lines from higher energies.

It is thus possible that the CO_2 and H_2O are being radiatively pumped by the hot dust, but this has not been directly observed. Note that all these species have strong electronic absorption bands at UV wavelengths which could be the source of the pumping through absorption of stellar radiation as well. Given the high column densities of these species, it would be interesting to investigate whether this could be a contributing source of the observed UV deficit in HR 4049 (Lamers et al. 1986). Formation pumping is certainly an appealing alternative, but is not well studied. While models exist for the formation pumping of H_2 after formation on dust grain surfaces (e.g., Gough et al. 1996; Takahashi & Uehara 2001), to our knowledge no such models exist for CO_2 or H_2O.

Finally, we note that while it appears that gas has been forming in the disk of HR 4049, the overall emitting surface does not seem to have changed significantly (remaining at $\sim$1300 AU^2). This agrees very well with the idea that the disk is relatively stable and long-lived (also supported by the unchanging CO overtone absorption observed between the observations of Lambert et al. 1988 and those by Hinkle et al. 2007).

Dominik et al. (2003) described how a gas-rich disk (such as the one we describe) would tend to settle toward the midplane and expand outward. Using a gas-to-dust ratio of 100 and an initial scale height of 4 AU, they estimated that the scale height of the disk would decrease by half in 150 yr. This effect could be mitigated by a higher gas-to-dust ratio and we suggest that the gas-to-dust ratio is likely to be greater than 100 in this environment. Indeed, if the dust is being slowly destroyed by stellar wind and gas is being formed, this ratio is likely to be increasing.

6. CONCLUSION

The *Spitzer*-IRS observations clearly reveal that the molecular gas in the circumbinary disk of HR 4049 is optically thick at infrared wavelengths and that the emission originates from a radially extended disk. The gas causes a strong greenhouse effect that plays a significant role in determining the thermal structure in the disk. Including the effect of optical depth, we determine that there is less of an enrichment in ^{17}O and ^{18}O than previously reported. Additionally, changes in the observed flux between *ISO* and *Spitzer* observations suggest ongoing chemical processing of oxygen-rich dust.

We acknowledge the support from the Natural Sciences and Engineering Research Council of Canada (NSERC). This work is based (in part) on observations made with the *Spitzer Space Telescope*, which is operated by the Jet Propulsion Laboratory, California Institute of Technology under a contract with NASA. This research has also made use of NASA's Astrophysics Data System Bibliographic Services and the SIMBAD database, operated at CDS, Strasbourg, France.

REFERENCES

Acke, B., Degroote, P., Lombaert, R., et al. 2013, A&A, 551, A76
Anders, E., & Grevesse, N. 1989, GeCoA, 53, 197
Bakker, E. J., Lambert, D. L., Van Winckel, H., et al. 1998, A&A, 336, 263
Bakker, E. J., van der Wolf, F. L. A., Lamers, H. J. G. L. M., et al. 1996, A&A, 306, 924
Beintema, D. A., van den Ancker, M. E., Molster, F. J., et al. 1996, A&A, 315, L369
Boersma, C., Bauschlicher, C. W., Allamandola, L. J., et al. 2010, A&A, 511, A32
Cami, J., Bernard-Salas, J., Peeters, E., & Malek, S. E. 2010a, Sci, 329, 1180
Cami, J., van Malderen, R., & Markwick, A. J. 2010b, ApJS, 187, 409
Cami, J., & Yamamura, I. 2001, A&A, 367, L1
Clayton, G. C., Geballe, T. R., Herwig, F., Fryer, C., & Asplund, M. 2007, ApJ, 662, 1220
de Graauw, T., Haser, L. N., Beintema, D. A., et al. 1996, A&A, 315, L49
Dominik, C., Dullemond, C. P., Cami, J., & van Winckel, H. 2003, A&A, 397, 595
Geballe, T. R., Noll, K. S., Whittet, D. C. B., & Waters, L. B. F. M. 1989, ApJL, 340, L29
Gielen, C., Bouwman, J., van Winckel, H., et al. 2011a, A&A, 533, A99
Gielen, C., Cami, J., Bouwman, J., Peeters, E., & Min, M. 2011b, A&A, 536, A54
Gielen, C., van Winckel, H., Matsuura, M., et al. 2009, A&A, 503, 843
Gielen, C., van Winckel, H., Min, M., Waters, L. B. F. M., & Lloyd Evans, T. 2008, A&A, 490, 725
Goorvitch, D. 1994, ApJS, 95, 535
Gough, S., Schermann, C., Pichou, F., et al. 1996, A&A, 305, 687
Guillois, O., Ledoux, G., & Reynaud, C. 1999, ApJL, 521, L133
Harris, M. J., & Lambert, D. L. 1984, ApJ, 285, 674
Harris, M. J., Lambert, D. L., Hinkle, K. H., Gustafsson, B., & Eriksson, K. 1987, ApJ, 316, 294
Harris, M. J., Lambert, D. L., & Smith, V. V. 1985a, ApJ, 292, 620
Harris, M. J., Lambert, D. L., & Smith, V. V. 1985b, ApJ, 299, 375
Harris, M. J., Lambert, D. L., & Smith, V. V. 1988, ApJ, 325, 768
Higdon, S. J. U., Devost, D., Higdon, J. L., et al. 2004, PASP, 116, 975
Hinkle, K. H., Brittain, S. D., & Lambert, D. L. 2007, ApJ, 664, 501
Hony, S., Van Kerckhoven, C., Peeters, E., et al. 2001, A&A, 370, 1030
Houck, J. R., Roellig, T. L., van Cleve, J., et al. 2004, ApJS, 154, 18
Iben, I., Jr., & Livio, M. 1993, PASP, 105, 1373
Justtanont, K., Tielens, A. G. G. M., de Jong, T., et al. 1999, A&A, 345, 605
Kessler, M. F., Steinz, J. A., Anderegg, M. E., et al. 1996, A&A, 315, L27
Lambert, D. L., Hinkle, K. H., & Luck, R. E. 1988, ApJ, 333, 917
Lamers, H. J. G. L. M., Waters, L. B. F. M., Garmany, C. D., Perez, M. R., & Waelkens, C. 1986, A&A, 154, L20
Lawson, C. L., & Hanson, R. J. 1974, Solving Least Squares Problems (Englewood Cliffs, NJ: Prentice Hall)
Lugaro, M., Pols, O., Karakas, A. I., & Tout, C. A. 2005, NuPhA, 758, 725
Malek, S. E., & Cami, J. 2013, ApJ, submitted
Malek, S. E., Cami, J., & Bernard-Salas, J. 2012, ApJ, 744, 16
Mathis, J. S., & Lamers, H. J. G. L. M. 1992, A&A, 259, L39
Molster, F. J., van den Ancker, M. E., Tielens, A. G. G. M., et al. 1996, A&A, 315, L373
Monier, R., & Parthasarathy, M. 1999, A&A, 341, 117
Moutou, C., Verstraete, L., Léger, A., Sellgren, K., & Schmidt, W. 2000, A&A, 354, L17
Partridge, H., & Schwenke, D. 1997, JChPh, 106, 4618
Peeters, E., Hony, S., Van Kerckhoven, C., et al. 2002, A&A, 390, 1089
Roberts, K. R. G., Smith, K. T., & Sarre, P. J. 2012, MNRAS, 421, 3277
Rothman, L. S., Gordon, I. E., Barbe, A., et al. 2009, JQSRT, 110, 533
Scott, P. C., Asplund, M., Grevesse, N., & Sauval, A. J. 2006, A&A, 456, 675
Smith, V. V., & Lambert, D. L. 1990, ApJS, 72, 387
Takada-Hidai, M. 1990, PASP, 102, 139
Takahashi, J., & Uehara, H. 2001, ApJ, 561, 843
Tashkun, S. A., Perevalov, V., Teffo, J. L., Bykov, A. D., & Lavrentieva, N. N. 2003, JQSRT, 82, 165
Tielens, A. G. G. M. 2008, ARA&A, 46, 289
Tielens, A. G. G. M., Hony, S., van Kerckhoven, C., & Peeters, E. 1999, in The Universe as Seen by ISO, ed. P. Cox & M. Kessler (ESA-SP: Vol. 427; Noordwijk: ESA), 579
Van Kerckhoven, C., Hony, S., Peeters, E., et al. 2000, A&A, 357, 1013
Van Winckel, H., Waelkens, C., & Waters, L. B. F. M. 1995, A&A, 293, L25
Waelkens, C., Lamers, H. J. G. L. M., Waters, L. B. F. M., et al. 1991a, A&A, 242, 433
Waelkens, C., Van Winckel, H., Bogaert, E., & Trams, N. R. 1991b, A&A, 251, 495
Waters, L. B. F. M., Lamers, H. J. G. L. M., Snow, T. P., et al. 1989, A&A, 211, 208
Waters, L. B. F. M., Trams, N. R., & Waelkens, C. 1992, A&A, 262, L37
Werner, M. W., Roellig, T. L., Low, F. J., et al. 2004, ApJS, 154, 1